Comparing microbubble cavitation at 500 kHz and 70 kHz related to micellar drug delivery using ultrasound

Mario A. Diaz de la Rosa [a], Ghaleb A. Husseini [b,⇑], William G. Pitt [a]

[a] Department of Chemical Engineering, Brigham Young University, Provo, UT 84602, United States

[b] Chemical Engineering Department, American University of Sharjah, Sharjah, United Arab Emirates

https://doi.org/10.1016/j.ultras.2012.07.004

Abstract

We have previously reported that ultrasonic drug release at 70 kHz was found to correlate with the presence of subharmonic emissions. No evidence of drug release or of the subharmonic emissions were detected in experiments at 500 kHz. In an attempt to understand the difference in drug release behavior between low- and mid-frequency ultrasound, a mathematical model of a bubble oscillator was developed to explore the difference in the behavior of a single 10-lm bubble under 500- and 70-kHz ultrasound. The dynamics were found to be fundamentally different; the 500-kHz bubble follows a period-doubling route to chaos while a 70-kHz bubble follows an intermittent route to chaos. We propose that this type of ''intermittent subharmonic'' oscillation behavior is associated with the drug release observed experimentally.

1. Introduction

In recent years, our research group has focused on studying the design of micelles that can be utilized in reducing the side effects of conventional chemotherapy [1–8]. One of the most important aspects of such design is optimizing the drug release which is achieved by choosing the optimal ultrasonic parameters (frequency, power density, pulse length, mechanical index, etc.). To achieve this goal, experimental measurements [5,9,10] as well as modeling techniques have been employed. The latter include two different mechanistic models to study the kinetics and thermodynamics of Doxorubicin (Dox) release from Pluronic P105 micelles [3,11,12], and artificial neural networks to capture the extent of release and to design model predictive controllers [13,14].

We have recently modeled the dynamic oscillation of bubbles under low frequency (70 kHz) ultrasound [15] in pursuit of a correlation between microbubble oscillations and drug release from Pluronic P105 micelles at 70 kHz. In the present paper, we extend our previous analysis to higher frequencies (namely 500 kHz) and embark on examining the possible reasons why micellar drug release from polymeric micelles was observed experimentally at lower frequencies (20 and 70 kHz), while such release was absent at 500 kHz. As with our previous publication [15], we use the Parlitz modification of the Keller–Miksis model to study bubble oscillations and dynamics at several acoustic amplitudes at 500 kHz and compare our results with those obtained at 70 kHz.

2. Experimental methods

2.1. Drug encapsulation in Pluronic unstabilized/stabilized micelles

Stock solutions of Pluronic (BASF, Mount Olive, NJ) were prepared by dissolving P105 in a PBS solution to a final concentration of 10 wt%. Doxorubicin (Dox) was obtained from the University of Utah Hospital (Salt Lake City, UT) in a 1:5 mixture with lactose and from Pharmacia & Upjohn Company (Kalamazoo MI), in dosage form; it was dissolved in phosphate buffered saline (PBS) and sterilized by filtration through a 0.2 lm filter. Dox was dissolved into the P105 solutions at room temperature to produce a final Dox concentration of 10 lg/ml in 10 wt% Pluronic. The same drug concentration was also prepared in PBS. The average size of the micelles was 10 ± 2 nm.

2.2. Ultrasound

Ultrasound (US) at 476 kHz (nominal 500 kHz) was applied using a focused transducer (H-104B, Sonic Concepts, Woodinville, WA). A sinusoidal waveform was generated using a function generator (HP 33120A, Hewlett–Packard) and amplified with a RF power amplifier (240L ENI, Rochester, NY). The signal was sent to the transducer from the amplifier through a matching network (Sonic Concepts, Woodinville, WA) to minimize reflected power. These experiments were carried out in an aluminum chamber (16 cm 13 cm 17.8 cm) filled with degassed water and containing acoustically absorbing rubber on the bottom and sides of the box in order to minimize reflections and standing waves.

2.3. Fluorescence detection

The apparatus previously used to measure drug release [4] was modified in order to capture fluorescence emission from a small volume (Fig. 1). A branch of a bifurcated fiber optic bundle directed a 488 nm beam of an argon ion laser (Ion Laser Technology, 5476 A) into a transparent (both optically and acoustically) plastic tube of cellulose butyrate containing the drug solution. Dox molecules absorbed the light at 488 nm and emitted fluorescent light between 530 and 630 nm. This emitted fluorescence was then captured by fibers in the fiber optic bundle and directed through its second branch to a silicon detector (EG&G 450–1). A dielectric bandpass filter (Omega Optical 535DF35) was used to eliminate emissions below 517 nm and above 552 nm. Finally, the signal from the photodetector was captured on an oscilloscope (Tektronix TDS 3012) and stored. The amount of drug release from the micelles was calculated from the data acquired by the system described above by using the same analysis as Husseini et al. [4]. It was assumed that the decrease in fluorescence of the solution was linearly related to the amount of drug released. Dox fluorescence at 100% release was approximated by the measured fluorescence of Dox in PBS while the Dox fluorescence at 0% release was approximated by the measured fluorescence of Dox in the carrier without the action of US.

To quantify the amount of drug released, the decrease in fluorescence after the drug was released from micelles was assumed to be directly proportional to the amount of the drug released relative to a known baseline. For instance, the fluorescence from the drug was measured in the absence of Pluronic to simulate 100% release into an aqueous solution. The percentage release was calculated using the following equation:

$$\%\ Release = \frac{I_{P105} - I}{I_{P105} - I_{PBS}}$$

In Eq. (1), I is the instantaneous fluorescence intensity, I_{PBS} refers to the fluorescence intensity recorded when the drug was introduced in a solution of PBS which corresponds to 100% release or no encapsulation, while I_{P105} refers to the intensity recorded when the drug was encapsulated in Pluronic P105 which corresponds to 0% release or 100% encapsulation. It is important to note that the fluorescence levels detected (I_{PBS}, I_{P105}, I) come primarily from the insonated area.

The experimental procedure is described below. First, the fluorescence intensity of the drug in PBS was measured both with and without ultrasound exposure, until no significant difference in the fluorescence intensity was observed; then, without changes in the experimental set-up, the PBS solution was carefully removed and replaced with the drug solution of the same concentration in Pluronic micelles. The new baseline fluorescence intensity was measured, after which CW or pulsed ultrasound was applied.

Since the US transducer at 500 kHz is focused, the most acoustically intense spot (or focal point) is unique and was carefully located before experiments began. The acoustic field of the transducer was mapped out with a calibrated needle hydrophone (HNR-1000, Onda, Sunnyvale, CA) mounted on a three axes micrometer stage. The drug-in-micelle samples were placed at the most acoustically intense site and the experiments proceeded as described previously [4]. Acoustic emissions from the samples were collected by the hydrophone placed 3 mm from the focal spot and laterally perpendicular to the axis of the transducer. Acoustic emissions were collected and Fourier-transformed to obtain the frequency spectra.

2.4. Monitoring radical formation

A collapse cavitation event is strong enough to produce free radicals whose rate of production can provide a quantifiable measure of collapse cavitation activity. The rate of OH radical formation under 500-kHz ultrasound was monitored by the reaction of hydroxyl radicals with iodide (I) ions in order to form iodine (I_2). A 70 mL solution of 0.03 wt% KI was sonicated for an hour with the same 500 kHz transducer described above at three different average intensities (374, 666, and 1040 W/cm^2) and circulated into a spectrophotometer (DU-640, Beckman Coulter, Fullerton, CA) which scanned the absorbance at 355 nm every fifteen seconds. This absorbance data was used to calculate a rate of iodine (and hence, hydroxyl radical) formation.

2.5. Mathematical model of a bubble oscillator

As previously described [15], we used the Parlitz modification of the Keller–Miksis model to study spherical bubble oscillation dynamics for the results presented in this paper. The equation is:

$$\left(1-\frac{\dot{R}}{c}\right)R\ddot{R}+\frac{3}{2}\dot{R}^2\left(1-\frac{\dot{R}}{3c}\right)=\left(1-\frac{\dot{R}}{c}\right)\frac{P}{\rho_L}+\frac{R}{\rho_L c}\dot{P}$$

where R is the bubble radius, c is the speed of sound in the liquid, and P is given by

$$P=(p_{stat}-p_v(T_\infty)+\frac{2S}{R_0})\left(\frac{R_0}{R}\right)^{3k}-\frac{2S}{R}-\frac{4\mu_L\dot{R}}{R}-p_{stat}+p_v(T_\infty)-A\sin(2\pi ft) \quad (3)$$

A is the acoustic pressure amplitude

We can now introduce the variables u = R− and Θ = ft mod 1 just as before to transform the Keller–Miksis–Parlitz equation into a system of three autonomous differential equations:

$$\dot{R}=u$$

$$\dot{u}=\left[\left(1-\frac{u}{c}\right)R+\frac{4\mu_L}{\rho_L c}\right]^{-1}\left[-\frac{u^2}{2}\left(3-\frac{u}{c}\right)+\left(1+(1-3k)\frac{u}{c}\right)\times\left(\frac{p_{stat}-p_v(T_\infty)}{\rho_L}+\frac{2S}{\rho_L R_0}\right)\left(\frac{R_0}{R}\right)^{3k}-\frac{2S}{\rho_L R}-\frac{4\mu_L}{\rho_L}\frac{u}{R}-\left(1+\frac{u}{c}\right)\times\frac{p_{stat}-p_v(T_\infty)+A\sin(2\pi\theta)}{\rho_L}-R\frac{2\pi f}{\rho_L c}A\cos(2\pi\Theta)\right]$$

$$\dot{\Theta}=f \quad (4)$$

More details on the bubble dynamic model, and its numerical solution were previously published [15].

The dynamics of this system were calculated using a Runga– Kutta routine in a standard MATLAB adaptive solver (ode45).

Our main goal was to model the bubble behavior and correlate it with the emissions observed experimentally. In particular, frequency spectra generated by the numerical solution of the bubble oscillator equations were compared to those found experimentally.

First the numerical models were integrated to obtain the bubble radii vs. acoustic pressure (orbit diagram trajectories) at various pressure amplitudes for a bubble with a 10-İm equilibrium bubble diameter.

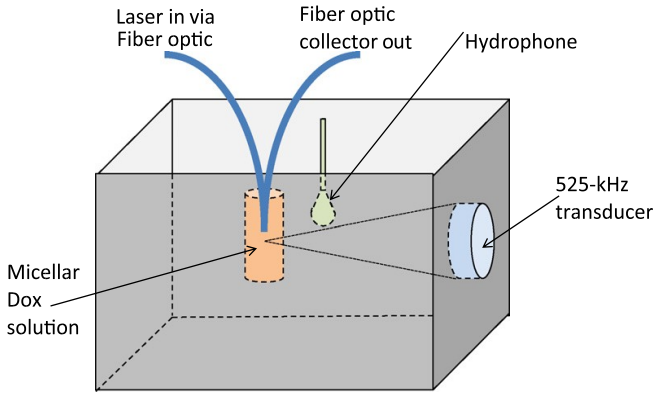

Fig. 1. Ultrasonic exposure chamber with fluorescence detection capable of simultaneously insonate micelles and collect acoustic and fluorescence emissions at 476 kHz.

To facilitate comparison with other data, the pressure amplitudes (A) are reported in terms of the mechanical index (MI) parameter, in which MI = (A/MPa)/(f/MHz)$^{1/2}$ [16–19]. The MI is often used by experimentalists and practitioners to estimate the probability and intensity of inertial cavitation [20–22]. To aid in visual comprehension of the numerical results, Poincar´e maps of the dynamic system were prepared [23]. Bifurcation values of the MI parameter and the resulting routes to chaos were identified and compared to the experimental values (both subharmonic and collapse cavitation thresholds).

3. Results

We have reported drug release from micelles subjected to low frequency ultrasound using a fluorescent technique [4,5,9,10]. The technique was based on an observed decrease of fluorescence when Dox was transferred from the hydrophobic core of P105 micelles to the surrounding aqueous solution. There was pronounced fluorescence decrease at 20 kHz, 45 kHz, 70 kHz and 90 kHz in the case of non-stabilized as well as stabilized micelles, indicating definite drug release [4,5,9,10]. However, no decrease in Dox fluorescence was detected at 476 kHz for intensities ranging from 0 to 20 W/cm^2 (MI from 0 to 1.1). Typical fluorescence profiles (at 476 and 70 kHz) are shown in Fig. 2. The lack of change in fluorescence indicates that Dox molecules remained in the hydrophobic environment provided by the core of the P105 micelles when exposed to 476 kHz ultrasound. This data implies that no Dox was released from P105 micelles at 476 kHz within this range of intensity. The decrease in fluorescence during the ‘‘ON’’ phase (at 70 kHz) suggests that the drug is released from the hydrophobic environment of Pluronic micellar cores into the aqueous environment, which may result from ultrasound-induced drug diffusion out of the micelles. Additionally, Fig. 2 (bottom) reveals the rapid re-encapsulation of the released drug during the ‘‘OFF’’ phase of ultrasound. This is an important finding because it indicates that non-internalized and non-extravasated (in the tumor) drug would re-enter the micelles and circulate in the encapsulated form upon leaving the sonicated volume, which will reduce unwanted drug interactions with normal tissues.

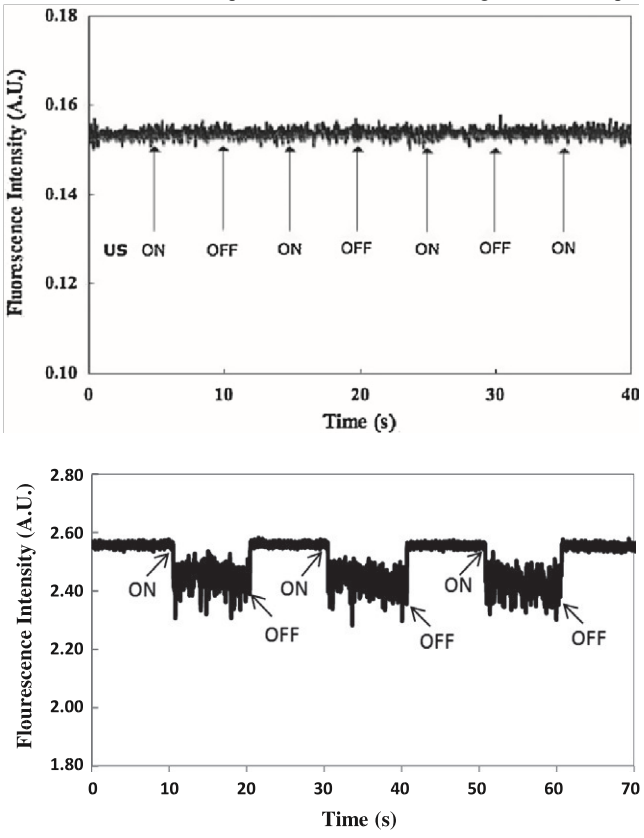

Fig. 2. Fluorescence of P105-encapsulated Dox (in arbitrary units) during 476-kHz (top) and 70-kHz sonication (bottom). Average intensity during the pulse is 20 W/cm^2.

Experimental acoustic spectra reveal the behavior of the bubbles by displaying the acoustic intensity as a function of frequency. For a group of bubbles driven at a given frequency f, it is expected that the strongest intensity reading will belong to f, the fundamental frequency. This behavior is seen in Fig. 3, a representative spectrum at 476 kHz and for an applied average intensity of 1.53 W/cm^2. As the applied intensity increases, the peak grows stronger and the baseline shifts up (Fig. 3, applied intensity of 195.8 W/cm^2). A shift in non-harmonic background emission is indicative of bubble collapse, which produces a shock wave emitting all frequencies. Harmonic (nf, n ϵ N) and a few ultraharmonic ((2n + 1) f/2, n ϵ N) peaks are present as well. A well-defined subharmonic peak, which is the signature most often associated with both stable and inertial cavitation, never appeared at any of the intensities used.

As was observed at lower frequencies, drug release was correlated with the magnitude of the subharmonic signal. However, the absence of subharmonic and of drug release was unexpected and prompted the subsequent numerical study of bubble behavior at 500 kHz.

For these experiments at 500 kHz, the highest intensity used (20 W/cm^2) corresponds to a mechanical index of 1.1, close to the limits of safe use. This means that, if higher intensities (than the ones used in this research) are indeed needed to release drug, they may not be of practical use in human therapy.

The high mechanical indices achieved in these experiments imply that inertial cavitation occurred, yet no drug was released. Inertial cavitation was verified by measuring hydroxyl radical generation which occurred at rates of 0.078, 0.112, and 0.120 İmol/h for the applied intensities of 374, 666, and 1040 W/cm^2, respectively. Hence, as the applied intensity increased, radical generation (i.e., bubble collapse events) also increased. These intensities correspond to mechanical indices of 4.74, 6.32, and 7.90, which are above the MI values of the release experiments. Radical monitoring and acoustic spectra suggest that, for sufficiently high intensities, bubble collapse occurs but the absence of an observable subharmonic signal raises doubts about the route followed by the bubbles to this eventual collapse. At 70 kHz a subharmonic signal and drug release were observed above a MI threshold of 0.37. Yet in the 500kHz experiments, the clear harmonic oscillations that preceded the sudden increase in broadband emissions reflect the stable oscillations of the bubbles in the system until the point of immediate inertial cavitation. It appears that the ultrasound that produces this type of bubble activity is unable to open Pluronic P105 micelles and release their therapeutic load. Therefore we undertook a comparison of bubble behavior at 500 kHz to that which occurs at 70 kHz and was associated with drug release.

The bubble dynamics equations generate the radial displacement and the bubble wall velocity as a function of time; representative time series are shown in Fig. 4 for a driving pressure, A, of 141.4 kPa, corresponding to a MI of 0.20. The solutions to the equations are analogous to acoustic emissions collected by the hydrophone during experiments and were similarly Fourier transformed to obtain the frequency spectra of the bubble oscillations.

The trajectories of any given initial conditions should trace a three-dimensional shape. The definition of the variable H leads to a convenient state space: the projection of the conic section traced by the smooth oscillations gives a torus like state space. Hence, the evolution of the variable H reflects the number of revolutions of a particular trajectory around this state space. One can then generate a projection of both R (radius) and u (bubble wall velocity), eliminating H and investigating the resulting phase portraits in two dimensions. The result is a limit cycle (an isolated closed trajectory) that appears (incorrectly) to cross itself, which is a consequence of the elimination of the extra dimension of time.

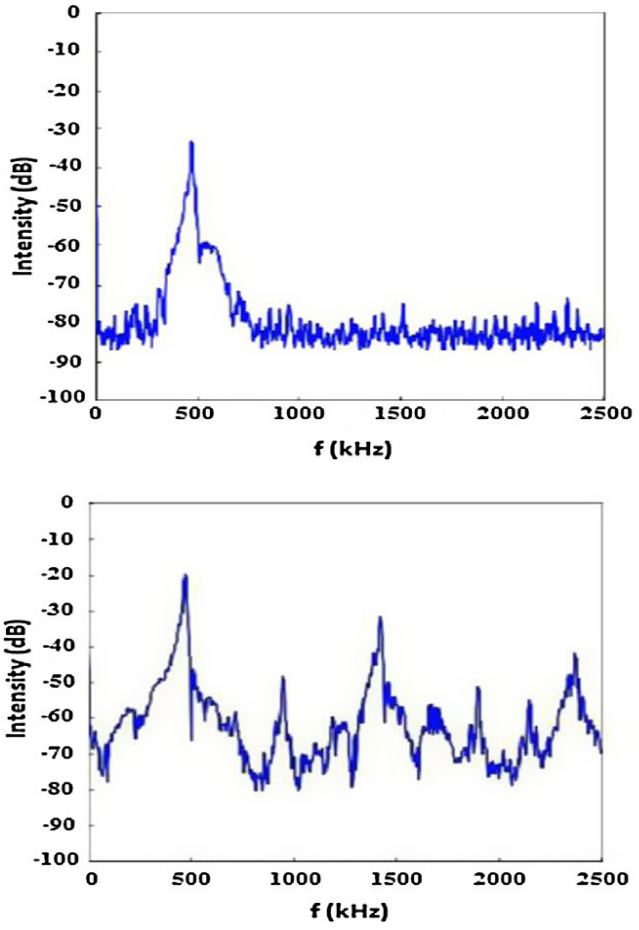

Fig. 3. Acoustic spectrum for 476 kHz insonation, I = 1.53 W/cm^2 and MI = 0.31 (top) and I = 195.8 W/cm^2 and MI = 3.51 (bottom). Fig. 3 acoustic spectrum for 476 kHz insonation, I = 195.8 W/cm^2.

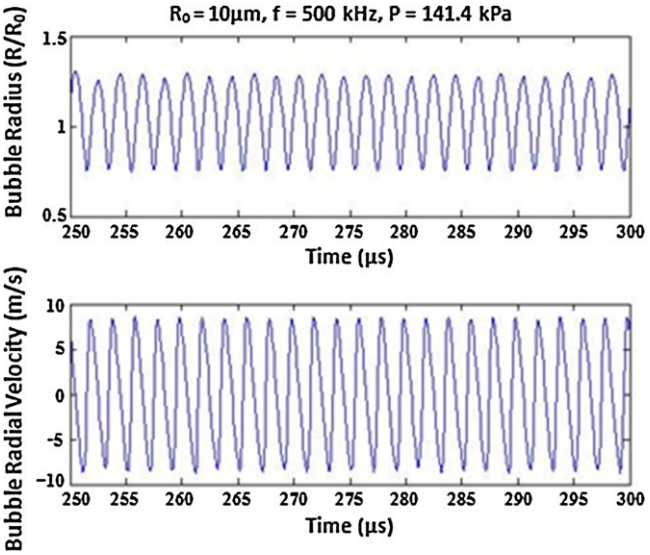

Fig. 4. Radius-time and velocity–time curves for MI = 0.20.

Additionally we employ the Poincar´e map from Strogatz [23]. The Poincar´e map is a important tool that allows one to move from the realm of continuous dynamic systems to the more intuitive world of discrete maps. However, it is difficult to find an explicit form of the map. Herein we rely on the numerical calculations of the ODE solver. Note that if x is a fixed point (i.e., P(x) = x), then a trajectory starting at x returns to x after some time T and is therefore a closed orbit for the original system x = f(x). Hence, when plotting the trajectories, any attracting limit cycles generated by the bubble equations will result in points on the Poincar´e map. If the bubble is oscillating at the driving frequency f, a single point should appear. If the bubble, however, has oscillations at twice the period of the applied pressure (that is to say, at half the frequency, f/2), then two points should appear on the Poincar´e map. In nonlinear dynamic systems (such as the one analyzed here), it is common to find another type of attractor, called a strange attractor. This is no longer a point, curve, or surface, but a fractal, and will reveal itself on the Poincar´e map as a type of ‘‘smearing’’ of points with self-similar structure [23–25].

The numerical simulation of bubble dynamics at 500 kHz follow a well-known dynamical pattern as the driving pressure increased. For low values of the applied pressure (in the case shown in Fig. 5, A = 106.1 kPa, corresponding to a MI of 0.15), the oscillations settle onto a stable limit cycle, a periodic orbit with a period equal to that of the driving pressure (Fig. 5a). Accordingly, we see a single point in the Poincar´e cross-section (Fig. 5b). This means that the acoustic spectrum should have a single peak at the driving frequency f = 500 kHz (Fig. 5c).

These oscillations are considered stable since they attract nearby initial conditions and because, as can be seen in Fig. 5a, the velocity remains uniform enough that the orbit traces a simple ellipse (no significant acceleration is seen as the bubble expands or contracts). The thickness of the cycle is due to the superposition of the curves traced by the orbit as it returns, in which curves do not exactly agree due to the numerical integration algorithm. Nevertheless, the cycle is stable, and this dynamic behavior persists until the bubble alters its period of oscillation.

At a pressure of about 195 kPa (MI 0.275), a second loop forms in the state space trajectory (Fig. 6a). The solution winds around once more before returning to the same point. This is clearly seen in the Poincar´e plot for this case (Fig. 6b), where another point appears, signifying the doubling of the period of oscillation (it takes the solution two driving periods to come back to the same point in space). One then expects the frequency spectrum to develop a subharmonic peak (at f/2 = 250 kHz), which is seen in Fig. 6c. This is a classic example of a period-doubling bifurcation of cycles.

Fig. 6a reveals more than just period doubling. It can be seen that the radial velocity begins to govern the dynamics of the bubble. While the maximum radius has only increased by about 25%, the maximum velocity (which occurs at low radii) has doubled, hence the slightly lopsided appearance of the cycle. While this is expected, it reveals the nonlinear nature of the oscillations, which becomes more evident as the accelerations, at the moment immediately preceding and following bubble collapse, increase dramatically.

The appearance of the subharmonic peak at this MI value is puzzling as this was not seen experimentally [4]. The biggest difference between the experiments and this model is, as mentioned above, the fact that only one bubble is modeled and the experimental frequency is slightly less than the simulation frequency. This could mean that bubble clouds at the parameters above inhibit double-period oscillations. This remains to be explored. Another possibility is that the experimental setup was not accurate enough to reach this particular parameter value. This is unlikely since this double period persists for a range of close to 1 unit of MI, as explained below. On the other hand, the hydrophone may not have been able to clearly register the subharmonic signal.

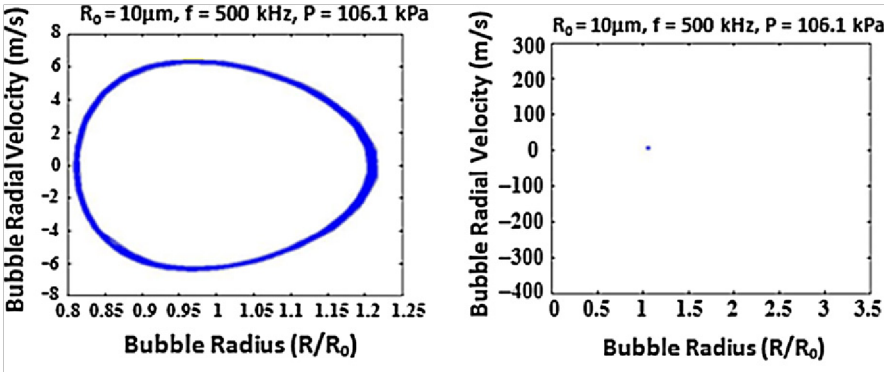

(a) Orbit, 500 kHz, $MI = 0.15$ (b) Poincaré, 500 kHz, $MI = 0.15$

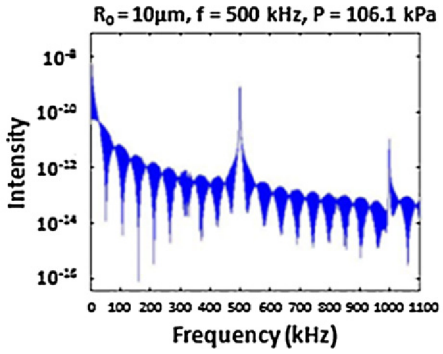

(c) FT, 500 kHz, $MI = 0.15$

Fig. 5. For a single 10 lm bubble at 500 kHz applied pressure and at a MI = 0.15: (a) trajectory in state space projection, (b) Poincar´e section plot, and (c) frequency spectrum.

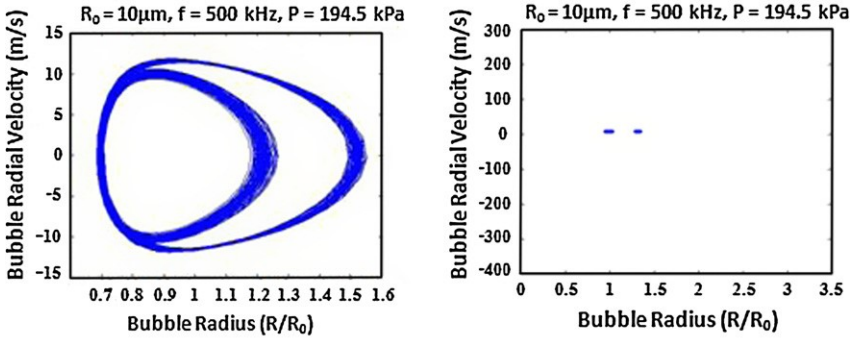

(a)Orbit, 500kHz, $MI = 0.275$ (b) Poincar´e,500kHz, $MI = 0.275$

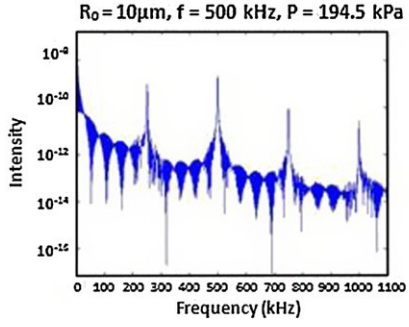

(c) Spectrum,500 kHz, $MI = 0.275$

Fig. 6. For a single 10 lm bubble at 500 kHz applied pressure and at a MI = 0.275: (a) trajectory in state space projection, (b) Poincar´e section plot, and (c) frequency spectrum

.

As stated above, the dynamics remain the same (double-period cycles) until a pressure of about 233 kPa is reached (MI 0.33), at which point a new period-doubling bifurcation of cycles is encountered. The orbit diagram in Fig. 7a does not explicitly show this new loop since it is so close to the original that it looks almost superimposed; but the Poincar´e section plot (Fig. 7b) shows the creation of two more points on the plane. Most importantly, the frequency spectrum shows peaks at f/4 = 125 kHz and its multiples
(Fig. 7c).

The funnel-type shape of the limit cycle shown in Fig. 7a contrasts with the one seen in Fig. 6a, which was rounder and smoother. The sharp acceleration at low radii reflects the bubble's increasingly violent behavior and foretells an impending collapse. A comparison of the spectrum in Fig. 7c with Fig. 6c reveals that, despite having undergone another period-doubling bifurcation, the base-line remains at the same level. This becomes important for subsequent MI values and in the context of the relationship between the subharmonic signal and non-harmonic background shift.

Having seen two period-doublings, we would like to know if this behavior continues on indefinitely. This is precisely the case. The orbit shown in Fig. 8a for an applied pressure of approximately 274 kPa (MI 0.875) reveals an increasingly complex trajectory which winds and twists ''within'' the projected orbit and stays preferentially at the highest velocities. Little can be gleamed from this orbit about the periods present at this pressure value, but the frequency spectrum (Fig. 8c) shows the clear emergence of a peak at f/8 = 62.5 kHz (and its multiples as ultraharmonics). The baseline has changed shape somewhat, becoming noisier and slightly leveling off the downward slope seen previously. This is most likely due to other frequencies that may be just outside the numerical accuracy in the spectrum but that start to appear as a curve on the Poincar´e cross-section (Fig. 8b), where no clear period 8 point can be seen.

It is important to mention at this point that the MI values reported become more and more approximate as numerical resolution decreases and it becomes increasingly difficult to find bifurcation thresholds. That said, it is indisputable that another period-doubling bifurcation has occurred around the MI value reported above. These are the signs of what is known in dynamic systems theory as the period-doubling route to chaos [26]. We speak now, in particular, of the Poincar´e map, which is a discrete map, since this ''route to chaos'' is defined for iterative maps of the line. We expect infinitely many periodic points in a chaotic regime (alternatively, all frequencies in the spectrum). This can only come from a strange attractor. Indeed, a small perturbation in MI at the f/8 threshold shown above creates a strange attractor.

A small step in applied pressure from 274 (MI = 0.3875) to 274.4 kPa (MI = 0.388) reveals the strange attractor that provides the infinitely many periodic points characteristic of a chaotic map. Fig. 9a shows the projection of this attractor, with its characteristic self-similar (fractal) structure, and is reminiscent of previous results in the literature that report on the chaotic attractors present in bubble dynamics [24,25]. As expected, the Poincar´e cross-section (Fig. 9b) appears as more of a smear of points that retain, however, some sense of structure. Strangely, contrary to what is expected, the whole fractal image does not seem to be traced out on the plane; it seems the numerical solution is not seeing some frequencies. More revealing, then, is the frequency spectrum shown in Fig. 9c. The baseline does not seem altered in any significant way (which is expected from the Poincar´e plot which fails to show all periods) but the appearance of third harmonics (f/3 and its multiples) stands out.

The peak at f/3 = 166.6 kHz in Fig. 9c means that we have, in the discrete sense of the Poincar´e map, a point of period three. Points of period three are important oddities in discrete dynamical systems, as expounded in the famous result of Sarkovskii. Consider the following ordering of N (known as Sarkovskii's ordering of the natural numbers):

$$3 \triangleright 5 \triangleright 7 \triangleright \cdots \triangleright 2\cdot 3 \triangleright 2\cdot 5 \triangleright \cdots \triangleright 2^2\cdot 3 \triangleright 2^2\cdot 5 \triangleright \cdots \triangleright 2^3\cdot 3 \triangleright 2^3\cdot 5 \triangleright \cdots \triangleright 2^3 \triangleright 2^2 \triangleright 2 \triangleright 1,$$

where all odd numbers (except 1) are listed first, followed by two times the odds, 2^2 times the odds, and so forth, leaving the powers of 2 for last, followed by 1. The theorem is:

Sarkovskii's Theorem. Let f R→ R be continuous. Suppose f has a periodic point of prime period k. If k Δ l in the above ordering, then f also has a periodic point of period l.

The theorem above is taken from Devaney [26], who also provides a basic proof. This theorem is remarkable for its simple hypothesis and strong result. The obvious corollary which concerns us is:

Corollary. Let f : R!R be continuous. Suppose f has a periodic point of period three. Then f has periodic points of all other periods.

Hence, by the Corollary above, if we restrict our Poincar´e map to the real line (by, for example, collapsing it onto the radius or velocity axis) and it is continuous, then a periodic point of period three implies the existence of points of all other periods. The theorem, however, says nothing about the stability of these points, and so while they may exist, they may not be stable and therefore invisible to the numerical algorithm, which is most likely the case here. The stability of these points can be expected to change upon perturbation, however, thereby revealing them in the solution to the differential equations.

For pressures higher than 274.4 kPa (MI > 0.388) the oscillations become obviously chaotic and in Fig. 10, we finally see the periods that were absent. The representative results for A = 495 kPa (MI = 0.70) are shown in Fig. 10. The beautiful self-similarity of the orbit is now clearly seen (Fig. 10a), while the Poincar´e crosssection (Fig. 10b) shows the fractal that we expected all along (notice that it shows a shape similar to the orbit). The frequency spectrum (Fig. 10c) now shows a noisy, raised baseline, a sign of the presence of all frequencies.

Thus we see that the dynamics of a 10-l̇m oscillating bubble with a driving frequency of 500 kHz follows the classic period-doubling route to chaos, starting at a MI of about 0.275. The oscillations reach chaos around MI = 0.388 and continue in the chaotic regime until at least a MI = 0.7. There are no stable regimes in this chaotic interval, except at MI 0.50 where a period three orbit is clearly seen again, implying a brief change in the stability of the infinitely many periodic points that masks them from the numerical solution.

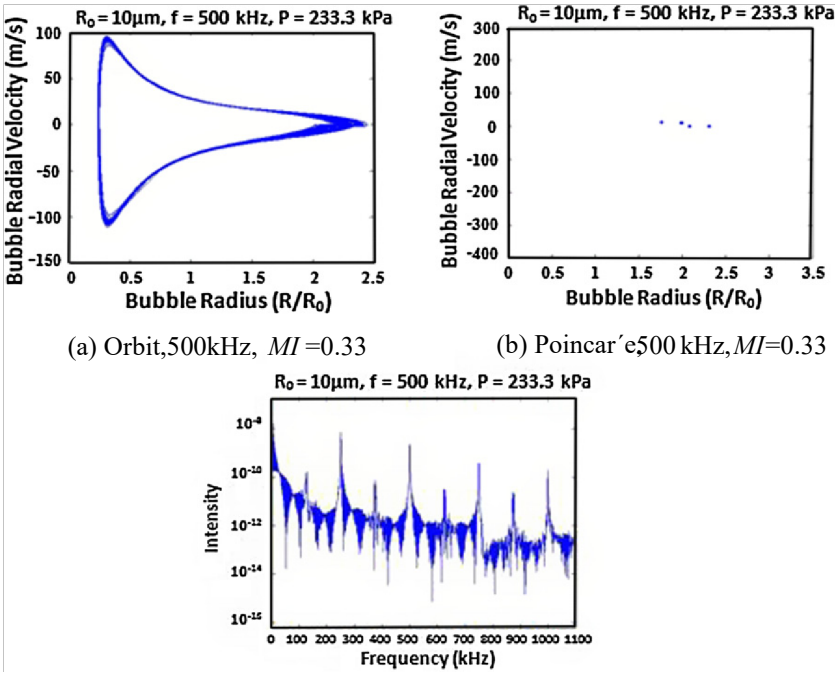

(a) Orbit,500kHz, *MI* =0.33 (b) Poincar´e,500 kHz, *MI*=0.33

(c) Spectrum,500 kHz, *MI* =0.33

Fig. 7. For a single 10 lm bubble at 500 kHz applied pressure and at a MI = 0.33: (a) trajectory in state space projection, (b) Poincar´e section plot, and (c) frequency spectrum.

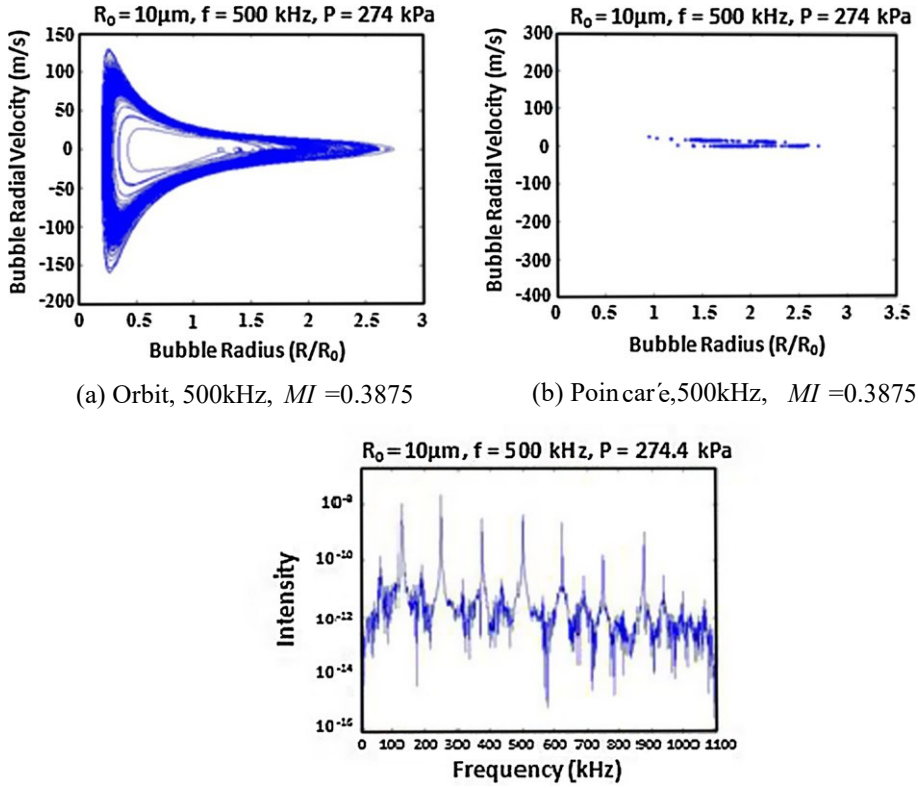

(a) Orbit, 500kHz, *MI* =0.3875 (b) Poincar´e,500kHz, *MI* =0.3875

(c) Spectrum, 500 kHz, *MI* = 0.3875

Fig. 8. For a single 10 lm bubble at 500 kHz applied pressure and at a MI = 0.3875: (a) trajectory in state space projection, (b) Poincar´e section plot, and (c) frequency spectrum.

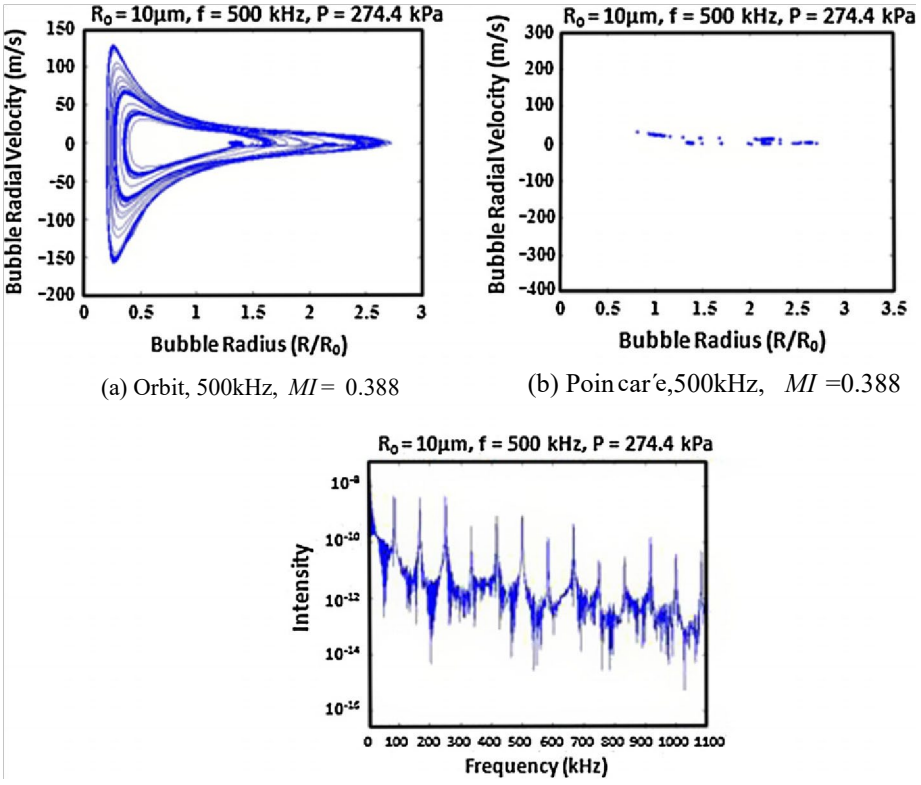

(a) Orbit, 500kHz, *MI* = 0.388

(b) Poincar´e,500kHz, *MI* =0.388

(c) Spectrum, 500 kHz,*MI* = 0.388

Fig. 9. For a single 10 lm bubble at 500 kHz applied pressure and at a MI = 0.388: (a) trajectory in state space projection, (b) Poincar´e section plot, and (c) frequency spectrum.

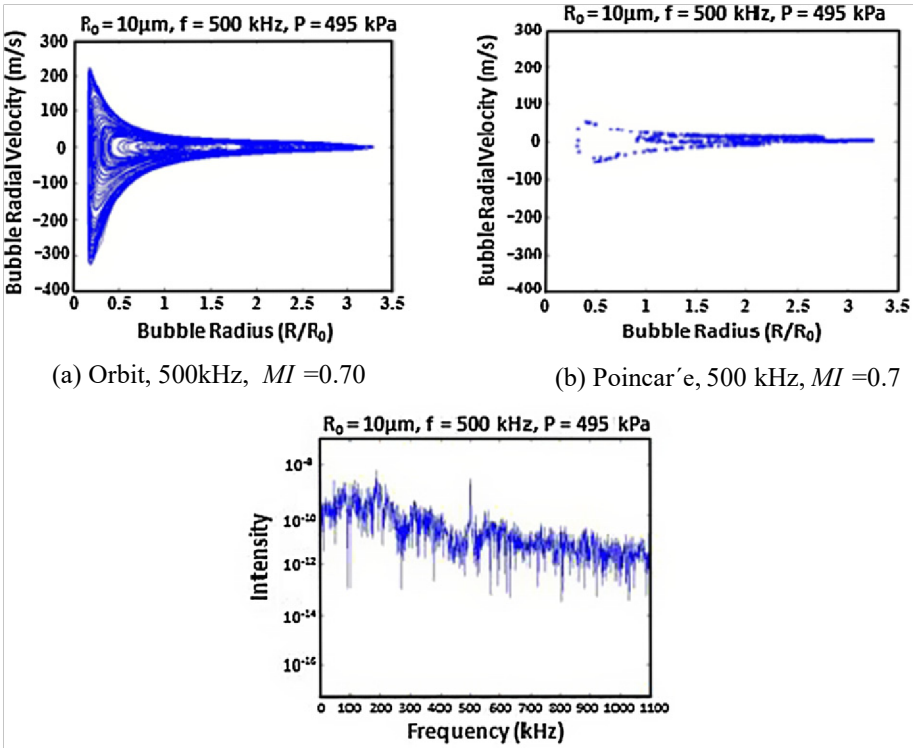

(a) Orbit, 500kHz, *MI* =0.70

(b) Poincar´e, 500 kHz, *MI* =0.7

(c) Spectrum, 500 kHz,*MI*= 0.70

Fig. 10. For a single 10 lm bubble at 500 kHz applied pressure and at a MI = 0.70: (a) trajectory in state space projection, (b) Poincar´e section plot, and (c) frequency spectrum.

4. Discussion

The dynamics of an oscillating bubble under the action of ultrasound are different between 70 and 500 kHz. This was expected since the system of equations of motion of bubble dynamics is a well-known chaotic dynamical system. But just how different and how does this relate to drug release from micelles? We previously published our findings using a bifurcation diagram at 70 kHz [15]. Here we discuss the same diagram at 500 kHz. One of our main observations at 70 kHz is the existence of discontinuities that may arise out of saddle-node bifurcations.

Having thus established the connection between the information presented by the bifurcation diagrams and the physical phenomena they represent, we can succinctly state the fundamental difference between bubble oscillations at 70 and 500 kHz: the bubble follows different routes to collapse. Interpreting the meaning of this statement proves rather difficult, however, but raises a number of interesting questions. The first, of course, is: what do we mean physically when we speak of a route to collapse?

The period-doubling route to chaos contrasts with the intermittent one in that it appears to be more gradual and deliberate than

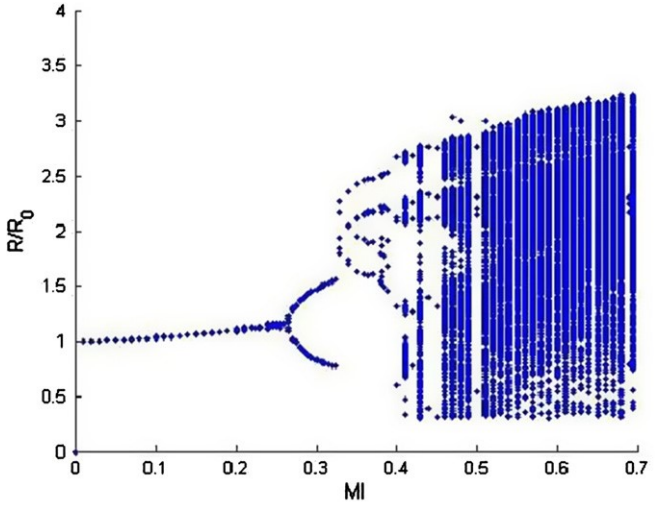

(a) Bifurcation Diagram for insonation f = 500kHz

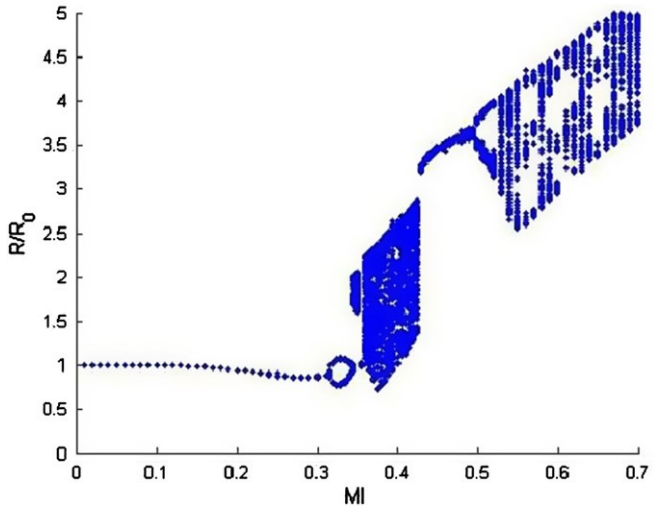

(b) Bifurcation Diagram for insonation at f = 70 kHz

Fig. 11. Bifurcation diagrams as a function of applied pressure for a 10 lm bubble at: (a) f = 500 kHz and (b) f = 70 kHz.

the intermittent movement between stable oscillations and sudden and erratic collapse. Another difference reported by Lauterborn and Parlitz [25] is the existence of hysteresis under the intermittent route to chaos (a testable phenomenon for future research). Additionally, the oscillations themselves appear to be quite different, with oscillations at 70 kHz more uneven and unstable than at 500 kHz (a possible consequence of resonance). It is possible that the forces that alter the structure of a micelle are produced only under the type of ''quasi-stable'' subharmonic oscillations seen at 70 kHz and that the transient and gradual perioddoublings at 500 kHz are insufficient for this effect.

It was hypothesized that bubble resonance played the defining role in the drastically different type of oscillations leading to collapse that were seen at the two frequencies. This provides future avenues of research rich in possibilities. Looking at the diagrams in Fig. 11 one must remember that they are but slices or projections of a highly complex multi-dimensional space. If we let the axis perpendicular to the plane shown represent the equilibrium bubble size R_0 and move along it, the resulting surface will reveal the effect of resonance we have discussed. For example, the small period-doubling window in Fig. 11b (0.32 6 MI < 0.35) could very likely change in radius as R_0 changes and affect the resulting route to chaos. Comparison of these predictions with experiments in which the bubble sizes present are carefully controlled would be the next natural step.

These routes to chaos must also be shown to occur experimentally. Period-doubling was not seen in the experiments conducted at 500 kHz, although the series of period-doublings could have been so fast as to avoid detection by the experimental system. Parlitz [27] recently presented a method to locate period-doubling and saddle-node bifurcations in experimental systems. Using these tools the presence of both routes to chaos could be confirmed for the experimental system directly. Conversely, an analytical approach to the problem will yield the conditions necessary to create the single (or series of) saddle-node bifurcation needed at 500 kHz for an intermittent route to chaos like the one witnessed at 70 kHz. In this case the tools of bifurcation theory (in particular, catastrophe theory) could be used to discover under which parameter values a fold in the geometry of parameter space could be reproduced at 500 kHz. Recorded drug release under such conditions would finally confirm that, indeed, the route to collapse followed by the bubbles is directly responsible for release.

Ultimately, drug release correlated with the subharmonic signal and not bubble collapse itself. It is easier in this case to speak of collapse since the difference in release for each frequency came down to a difference in approaches to collapse. It is the subharmonic, however, that still holds the elusive answer.

5. Conclusions

This research has produced four primary conclusions: (1) drug release from Pluronic micelles occurs at 70 kHz, but not at 500 kHz; (2) drug release correlates with the experimental subharmonic signal at 70 kHz; (3) it also correlates with the experimental subharmonic when 500 kHz is applied in that neither subharmonic nor drug release is observed; and (4) inertial bubble collapse is not a sufficient requirement for drug release at either frequency. Such apparent paradoxes only serve to add to the confusion already present in the long-ongoing stable vs. collapse cavitation debate. Actually, however, what these findings reveal is that we have been asking the wrong questions all along. The chaotic nature of bubble dynamics shows that our physical interpretation of bubble oscillations cannot possibly remain within the oversimplified rubric of ''stable'' or ''inertial.'' Indeed, our definition and categorization of cavitation must be updated to include cases analogous to all the dynamic states present in this complex dynamical system, including, but not limited to, the two distinct routes to chaos here discussed. The meaning of mechanical index may have to be similarly reevaluated as well. Admittedly, in order to fully define all types of cavitation, parameter space must be explored fully (a herculean task, to say the least). In the present case, it can at least be said that drug release requires and correlates with a type of ''intermittent subharmonic'', but our numerical modeling suggests that it does not correlate with the ''cascade subharmonic'' associated with the period-doubling route to chaos.

Acknowledgments

The authors would like to acknowledge funding from the National Institutes of Health (R01 CA-98138), the Pope Professorship at Brigham Young University, and the Faculty Research Grant at the American University of Sharjah (FRG-AUS10).

References

[1] G.A. Husseini, R.I. El-Fayoumi, K.L. O'Neill, N.Y. Rapoport, W.G. Pitt, DNA damage induced by micellar-delivered doxorubicin and ultrasound: comet assay study, Cancer Lett. 154 (2000) 211–216.

[2] G.A. Husseini, K.L. O'Neill, W.G. Pitt, The comet assay to determine the mode of cell death for the ultrasonic delivery of doxorubicin to human leukemia (HL-60 cells) from pluronic P105 micelles, Technol. Cancer Res. Treat. 4 (2005) 707– 711.

[3] G.A. Husseini, N.Y. Rapoport, D.A. Christensen, J.D. Pruitt, W.G. Pitt, Kinetics of ultrasonic release of doxorubicin from Pluronic P105 micelles, Colloid Surf. B: Biointerfaces 24 (2002) 253–264.

[4] G.A. Husseini, M.A. Diaz, E.S. Richardson, D.A. Christensen, W.G. Pitt, The role of cavitation in acoustically activated drug delivery, J. Control. Release 107 (2005) 253–261.

[5] G.A. Husseini, M.A. Diaz de la Rosa, T. Gabuji, Y. Zeng, D.A. Christensen, W.G. Pitt, Release of doxorubicin from unstabilized and stabilized micelles under the action of ultrasound, J. Nanosci. Nanotech. 7 (2007) 1–6.

[6] B.J. Staples, B.L. Roeder, G.A. Husseini, O. Badamjav, G.B. Schaalje, W.G. Pitt, Distribution of doxorubicin in rats subjected to ultrasonic cancer therapy, J. Pharm. Sci. 99 (7) (2010) 3122–3131.

[7] S.B. Stringham, M.A. Viskovska, E.S. Richardson, S. Ohmine, G.A. Husseini, B.K. Murray, W.G. Pitt, Over-pressure suppresses ultrasonic-induced drug uptake, Ultras. Med. Biol. 35 (2009) 409–415.

[8] B.J. Staples, B.L. Roeder, G.A. Husseini, O. Badamjav, G.B. Schaalje, W.G. Pitt, Role of frequency and mechanical index in ultrasonic-enhanced chemotherapy in rats, Cancer Chemother. Pharmacol. 64 (2009) 593–600.

[9] G.A. Husseini, G.D. Myrup, W.G. Pitt, D.A. Christensen, N.Y. Rapoport, Factors affecting acoustically-triggered release of drugs from polymeric micelles, J. Control. Release 69 (2000) 43–52.

[10] G.A. Husseini, D.A. Christensen, N.Y. Rapoport, W.G. Pitt, Ultrasonic release of doxorubicin from Pluronic P105 micelles stabilized with an interpenetrating network of N,N-diethylacrylamide, J. Control. Release 83 (2002) 302–304.

[11] D. Stevenson-Abouelnasr, G.A. Husseini, W.G. Pitt, Further investigation of the mechanism of Doxorubicin release from P105 micelles using kinetic models, Colloids Surf. B-Biointerfaces 55 (2007) 59–66.

[12] G.A. Husseini, D. Stevenson-Abouelnasr, W.G. Pitt, K.T. Assaleh, L.O. Farahat, J. Fahadi, Kinetics and thermodynamics of acoustic release of doxorubicin from non-stabilized polymeric micelles, Colloids Surf. A-Physicochem. Eng. Aspects 359 (2010) 18–24.

[13] G.A. Husseini, N.M. Abdel-Jabbar, F.S. Mjalli, W.G. Pitt, Modeling and sensitivity analysis of acoustic release of Doxorubicin from unstabilized pluronic P105 using an artificial neural network model, Technol. Cancer Res. Treat. 6 (2007) 49–56.

[14] G.A. Husseini, F.S. Mjalli, W.G. Pitt, N.M. Abdel-Jabbar, Using artificial neural networks and model predictive control to optimize acoustically assisted doxorubicin release from polymeric micelles, Technol. Cancer Res. Treat. 8 (2009) 479–488.

[15] M.A. Diaz de la Rosa, G.A. Husseini, W.G. Pitt, Numerical simulations of microbubble cavitation at 70 kHz and the importance of the subharmonic in drug delivery from micelles, Ultrasonics 53 (2012) 97–110.

[16] S. Daniels, D. Blondel, L.A. Crum, G.R. ter Haar, M. Dyson, Ultrasonically induced gas bubble production in agar based gels: Part I, experimental investigation, Ultras. Med. Biol. 13 (1987) 527–539.

[17] M. Delius, Minimal static excess pressure minimises the effect of extracorporeal shock waves on cells and reduces it on gallstones, Ultras. Med. Biol. 23 (1997) 611–617.

[18] C.C. Church, Frequency, pulse length, and the mechanical index, Acoustics Research Letters Online-Arlo 6 (3) (2005) 162–168.

[19] Z. Ding, S.M. Gracewski, Response of constrained and unconstrained bubbles to lithotripter shock wave pulses, J. Acoust. Soc. Am. 96 (1994) 3636–3644.

[20] R.E. Apfel, C.K. Holland, Gauging the liklihood of cavitation from short-pulse, low-duty cycle diagnostic ultrasound, Ultras. Med. Biol. 17 (1991) 179–185.

[21] S. Barnett, Thresholds for nonthermal bioeffects: theoretical and experimental basis for a threshold index, Ultras. Med. Biol. 24 (1998) S41–S49.

[22] S.B. Barnett, G.R.T. Haar, M.C. Ziskin, H.-D. Rott, F.A. Duck, K. Maeda, International recommendations and guidelines for the safe use of diagnostic ultrasound in medicine, Ultras. Med. Biol. 26 (2000) 355–366.

[23] S.H. Strogatz, Nonlinear Dynamics and Chaos, Perseus, Cambridge, MA, 1994.

[24] U. Parlitz, V. Englisch, C. Scheffczyk, W. Lauterborn, Bifurcation structure of bubble oscillators, J. Acoust. Soc. Am. 88 (1990) 1061–1077.

[25] W. Lauterborn, U. Parlitz, Methods of chaos physics and their applications to acoustics, J. Acoust. Soc. Am. 84 (1988) 1975–1993.

[26] R.L. Devaney, An Introduction to Chaotic Dynamical Systems, second ed., Westview Press, Boulder, CO, 2003.

[27] U. Parlitz, Robust method for experimental bifurcation analysis, Int. J. Bifurcat. Chaos 12 (2002) 1909–1913.